but does not allow the resolution of the 50–60-eV peak of the (01) beam into the double-peak structure seen in the experimental curve. A similar instance was noted in Sec. IV for the (10) beam of the aluminum (110) surface in the same energy region. Discrepancies in the low-energy ($\lesssim 50$ eV) peak positions for the (111) surface are of the same magnitude as those observed with the (110) surface and indicate that such effects are attributable to the form of the ion-core potential, or to the model employed for the complex electron self-energy rather than to the geometrical arrangement of the crystal layers in the surface region.

ACKNOWLEDGMENTS

This work was supported by the U. S. Atomic Energy Commission. The authors are grateful to Dr. J. B. Pendry for supplying the computer program used to calculate the ion-core phase shifts.

[1]J. B. Pendry, J. Phys. C **2**, 2273 (1969); J. Phys. C **2**, 2283 (1969).
[2]G. Capart, Surf. Sci. **26**, 429 (1971).
[3]J. A. Strozier, Jr. and R. O. Jones, Phys. Rev. B **3**, 3228 (1971).
[4]J. L. Beeby, J. Phys. B **1**, 82 (1968).
[5]C. B. Duke and C. W. Tucker, Jr., Surf. Sci. **15**, 231 (1969).
[6]C. B. Duke, J. R. Anderson, and C. W. Tucker, Jr., Surf. Sci. **19**, 117 (1970).
[7]D. W. Jepsen, P. M. Marcus, and F. Jona, Phys. Rev. Lett. **26**, 1365 (1971); Phys. Rev. B **5**, 3933 (1972).
[8]D. W. Jepsen and P. M. Marcus, *Computational Methods in Band Theory* (Plenum, New York, 1971), p. 416.
[9]S. Y. Tong and T. N. Rhodin, Phys. Rev. Lett. **28**, 553 (1972).
[10]R. H. Tait, S. Y. Tong, and T. N. Rhodin, Phys. Rev. Lett. **28**, 553 (1972).
[11]J. B. Pendry, Phys. Rev. Lett. **27**, 856 (1971).
[12]G. E. Laramore and C. B. Duke, Phys. Rev. B **2**, 4782 (1970).
[13]C. W. Tucker, Jr. and C. B. Duke, Surf. Sci. **24**, 31 (1971).
[14]J. B. Pendry, J. Phys. C **4**, 3095 (1971).
[15]E. C. Snow, Phys. Rev. **158**, 683 (1967); Phys. Rev. **171**, 785 (1968).
[16]J. B. Pendry, J. Phys. C **4**, 2501 (1971).
[17]G. E. Laramore and C. B. Duke, Phys. Rev. B **5**, 267 (1972).
[18]G. E. Laramore, C. B. Duke, A. Bagchi, and A. B. Kunz, Phys. Rev. B **4**, 2058 (1971).
[19]J. B. Pendry (private communication).
[20]P. M. Marcus, D. W. Jepsen, and F. Jona, Surf. Sci. **31**, 180 (1972).
[21]F. Jona, IBM J. Res. Dev. **14** (4), ,(1970).
[22]B. I. Lundqvist, Phys. Status Solidi **32**, 273 (1969).
[23]G. E. Laramore, J. E. Houston, and R. L. Park (to be published).
[24]N. D. Lang and W. Kohn, Phys. Rev. B **3**, 1215 (1971).

PHYSICAL REVIEW B VOLUME 7, NUMBER 8 15 APRIL 1973

Low-Energy-Electron-Diffraction Intensity Profiles and Electronic Energy Bands for Lithium Fluoride*

G. E. Laramore and A. C. Switendick
Sandia Laboratories, Albuquerque, New Mexico 87115
(Received 4 October 1972)

Model calculations of the low-energy-electron-diffraction (LEED) intensity profiles for LiF (100) and of the bulk electronic energy bands for LiF are performed using model potentials with quite different degrees of ionicity. One potential is constructed using Li^0 and F^0 free-atom charge densities and the other is constructed using Li^+ and F^- free-ion charge densities. Although both model potentials yield rather similar band gaps, the photoemission threshold and LEED measurements clearly favor the Li^+F^- form of the potential. Experimental LEED intensity profiles for LiF (100) at $T = 573$ °K are analyzed, and certain features strongly suggest that the top lithium and fluorine sublayers do not lie in the same plane but are separated by about 0.25 Å in a direction normal to the surface. In order to motivate further experimental work, additional intensity profiles are calculated for both the perfect surface model and the reconstructed surface model.

I. INTRODUCTION

Thus far, all low-energy-electron-diffraction (LEED) calculations utilizing a microscopic model for the electron–ion-core potential have dealt with scattering from metal surfaces. In spite of the complete neglect of the effects of surface morphology and the use of bulk electron–ion-core potentials, in many instances these calculations have achieved a reasonable correspondence with experimental measurements of LEED intensities.[1–9] However, the intrinsic interest in LEED as a tool

for surface structural analysis lies not in describing the scattering data from clean metal surfaces where the geometrical parameters appear to differ little from bulk values. The hope is that we can use it to learn about surface reconstruction in elemental materials and about the structural properties of absorbed overlayers. Some of the complicated spot patterns that have been observed in such instances may be found in the review articles of May[10] and Estrup and McRae.[11] Although data-averaging techniques hold considerable promise for obtaining the geometrical parameters for such structures,[12–15] the errors introduced by uncertainties in the effective electron–ion-core scattering amplitude for the surface atoms (e.g., due to vibronic and charge-transfer effects) have not been clearly assessed. These uncertainties, of course, affect the interpretation of microscopic calculations of LEED intensity profiles, but a direct comparison between theoretical intensity profiles using different model potentials and experimental measurements allows us to estimate the importance of various aspects of the potential construction.

In this paper we make a logical next step in applying the theoretical models to increasingly more complex systems and calculate LEED intensity profiles from a two-component system. The system chosen was the (100) face of LiF because of the experimental work of McRae and Caldwell.[16] To our knowledge this is also the first instance where a calculation utilizing a microscopic model for the electron–ion-core potential has been applied to an insulator. We compare our results with calculations by Hirabayashi[17] and Holland *et al.*[18] which use only s-wave scattering to model the electron–ion-core interaction to assess the importance of using a more realistic model potential. Another question that we consider is the importance of using the correct charge states[19,20] for the component species in constructing the effective electron–ion-core potentials. Two sets of muffin-tin potentials were constructed—one using neutral-atom charge densities and the other Li^+ and F^- free-ion charge densities as a starting point. In addition to the LEED intensity profiles, the low-lying electronic energy-band structure was calculated by the augmented-plane-wave (APW) method.[21,22] The energy bands are compared with the results of previous calculations[23–26] for LiF. The predicted band gaps are compared with experimental optical and electron energy-loss data as interpreted in Ref. 23 and the positions of the valence bands relative to the vacuum are compared with the photoemission threshold.[27] Although the experimental band gaps appear to agree somewhat better with the results of the neutral-atom model, both the photoemission data and the LEED measurements strongly favor the Li^+F^- model. The sensitivity of the calculated LEED intensity profiles to this feature of the model potential indicates that taking into account the charge transfer between the adsorbate and the substrate will be quite important in constructing potentials for adsorbed-overlayer systems. It is encouraging, though, to note that Andersson and Pendry[6] have satisfactorily modeled LEED data for the substrate beams in the 0–40-eV range for a sodium $c(2\times2)$ overlayer on Ni (100).

The surface properties of the alkali halides are also an interesting study in their own right. Calculations of the surface relaxation of these materials have been performed by Benson *et al.*[28–30] They find that a separation between the anion and cation species in the upper layers can occur in the (100) faces of these materials, i.e., one species experiences a greater degree of relaxation than the other. Unfortunately, the convergence properties of the calculation appear questionable for LiF.[29,30] We find that certain features of the LEED intensity profiles strongly suggest that the Li^+ and F^- subplanes in the top layer are separated by about 0.25 Å at 573 °K. Relative to the perfect-crystal layer spacing, the top fluorine sublayer is contracted about 0.1 Å towards the bulk and the top lithium sublayer is contracted about 0.35 Å towards the bulk.

In Sec. II we discuss the construction of the muffin-tin potentials used in the calculation and present the phase shifts that are used in the LEED intensity calculations. In Sec. III we show the low-lying energy bands for each set of potentials. In Sec. IV we briefly discuss the vibronic and electronic renormalization effects that must be taken into account in using these potentials in a LEED calculation. In Sec. V we present our calculated LEED intensity profiles and compare them with experimental results. The effect of various surface relaxation phenomena on the calculated intensity profiles is also shown. Finally, in Sec. VI we summarize our results.

II. ELECTRON–ION-CORE MODEL POTENTIALS

The electron–ion-core potentials used in this work were constructed assuming a three-dimensional geometrical configuration corresponding to a perfect crystal. Atomic or ionic charge densities were obtained from a nonrelativistic calculation following Herman and Skillman.[31] In the case of the Li^0F^0 starting configuration the atomic charge densities were overlapped and a muffin-tin potential for each species was constructed in the usual way.[22] In the case of the Li^+F^- starting configuration the free-ion charge densities were overlapped, and a Madelung correction term accounting for the electrostatic field of the ions in the lattice structure was included.[23,32] The Slater[33] local exchange approximation

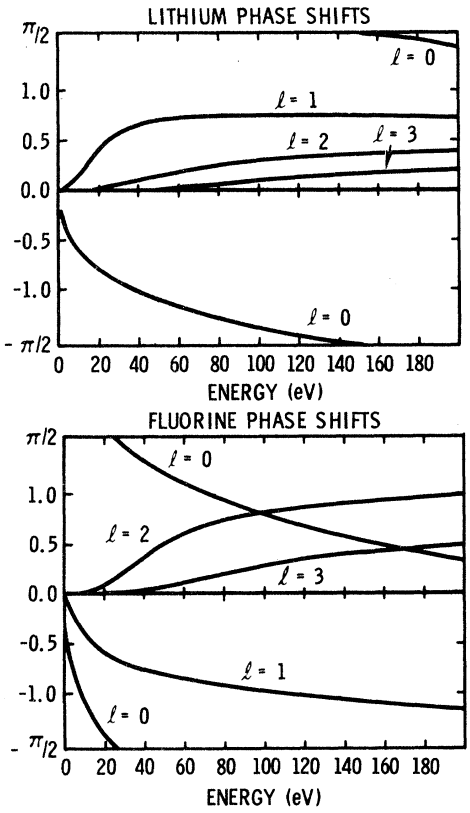

FIG. 1. Phase shifts obtained from the muffin-tin potential constructed from a Li^0F^0 starting configuration (model potential I). The energy scale is measured relative to the constant value of the potential between the muffin tins. This zero level is 18 eV below the vacuum level.

$$V_{\text{exch}}(r) = -6\alpha[(3/8\pi)\rho(r)]^{1/3} \quad (1)$$

was used with $\alpha = 1$ both in the Herman–Skillman calculations and in the muffin-tin construction. The average exchange potential outside the APW spheres was calculated using the average exterior charge density. The muffin-tin radii were taken as 1.73 a.u. for lithium and 2.01 a.u. for fluorine for both the neutral-atom and the ionic configurations with the nearest-neighbor distance equal to 3.80 a.u. These are the same values as used by Page and Hygh.[23] Nonspherical corrections to the potentials were not taken into account.

The most striking difference between the two sets of potentials is in the position of the muffin-tin zero relative to the vacuum. For the Li^0F^0 starting configuration (model I), the muffin-tin zero is about 18 eV below the vacuum, and for the Li^+F^- starting configuration (model II), the muffin-tin zero is about 11.6 eV below the vacuum.

We require the scattering phase shifts with the energy scale defined relative to the muffin-tin zero to calculate the LEED intensities. These are shown for the two sets of potentials in Figs. 1 and 2. There are only slight differences between these two sets of phase shifts.

III. ELECTRONIC ENERGY BANDS

Electronic energy bands were calculated by the APW method[21,22] for the two sets of muffin-tin potentials described in Sec. II. These energy bands are shown in Figs. 3 and 4. In general appearance these two sets of energy bands are quite similar but are shifted with respect to one another owing to the different values of the muffin-tin zero. The band gaps for each set of potentials are shown in Table I, where they are compared with experimentally observed transitions.[23] Although the

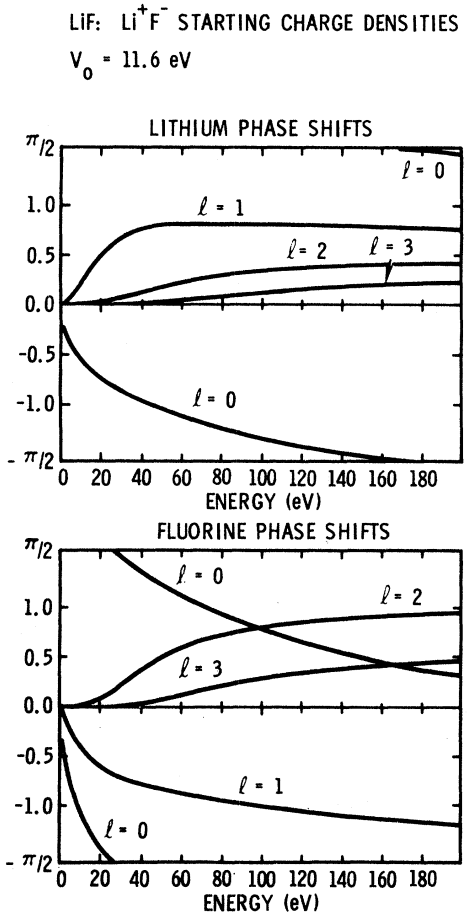

FIG. 2. Phase shifts obtained from the muffin-tin potential constructed from a Li^+F^- starting configuration (model potential II). The energy scale is measured relative to the constant value of the potential between the muffin tins. This zero level is 11.6 eV below the vacuum level.

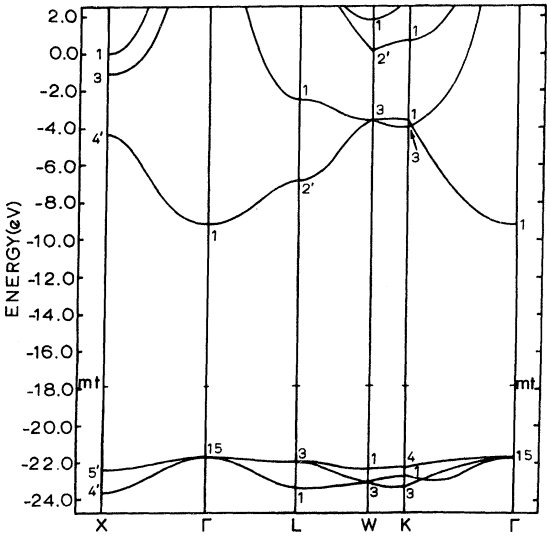

FIG. 3. Energy bands for LiF using a muffin-tin potential constructed from a Li^0F^0 starting configuration (model potential I). The electron energies are given in eV relative to the vacuum level. mt denotes the position of the muffin-tin zero.

TABLE I. Comparison between theoretical band gaps for each potential model and experimental observations. The energy values are given in eV.

			Experiment[c]		
	Potential I[a]	Potential II[b]	A	B	C
$\Gamma_{15}\rightarrow\Gamma_1$	12.55	11.27	<14.0	13.6	13.5
$L_3\rightarrow L_2$	15.06	13.66	15.6	14.3	16.0
$X_{5'}\rightarrow X_{4'}$	17.97	17.07	17.8	17.4	18.0
$L_3\rightarrow L_1$	19.44	18.46	20.75	21.7	21.5
$X_{5'}\rightarrow X_3$	21.33	20.13	22.6	23.0	24.4
$X_{5'}\rightarrow X_1$	22.38	20.79	23.9		

[a]Potential constructed from Li^0F^0 starting configuration.

[b]Potential constructed from Li^+F^- starting configuration.

[c]Experimental data as interpreted in Ref. 23. Column A is Ref. 34, Col. B is Ref. 35, and Col. C. is Ref. 36.

scatter between the different experimental measurements is of order 1 eV (which is the same order of magnitude as the differences between the two model potentials), on balance model I is favored by the experimental observations. However, the experimental photoemission threshold[27] lies near 12 eV and this determines the top of the valence band relative to the vacuum level. In Fig. 3 the top of the valence band lies 21.8 eV below the vacuum and in Fig. 4 the top of the valence band lies 14.3 eV below the vacuum. This clearly favors potential model II. The valence band is quite flat for each potential model and so it is the difference between the muffin-tin zeros which gives rise to the large variation between the two models. In Sec. V we shall see that it is this distinguishing feature which causes the LEED measurements to favor model II. Since there have been several previous band calculations of LiF [23–26] using different potentials and different methods (and obtaining different quantitative results), we shall try to critically evaluate the sources of these differences.

APW energy bands for LiF have been previously calculated by Page and Hygh.[23] They started with Li^+F^- free-ion charge densities and took α in Eq. (1) as an adjustable parameter. They also took certain nonspherical terms in the potential into account in a perturbative sense. The inclusion of the nonspherical terms had the effect of lowering the calculated conduction bands by amounts varying between about 0.4 and 1.3 eV. Page and Hygh[23] did not give the value of α corresponding to their best fit to the experimental data or the position of the muffin-tin zero below the vacuum. The general appearance of their energy bands is quite similar to that of the bands shown in Figs. 3 and 4. Detailed quantitative agreement is lacking even when their nonspherical corrections are considered. A value of α somewhat greater than 1 is implied by these differences since their muffin-tin potential should be the same as our model-II potential. [Their Eq. (6) using superimposed free-ion charge densities would appear to be counted twice in their Eq. (4).]

Chaney *et al.*[24] calculated the LiF energy bands

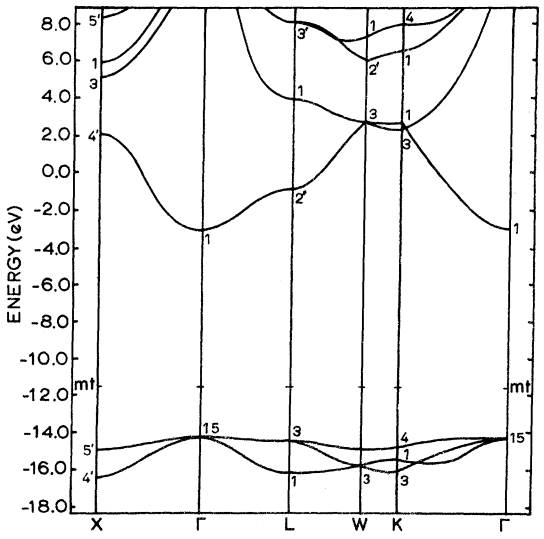

FIG. 4. Energy bands for LiF using a muffin-tin potential constructed from a Li^+F^- starting configuration (model potential II). The electron energies are given in eV relative to the vacuum. mt denotes the position of the muffin-tin zero.

by the tight-binding method. Their bands exhibit the same general trends as ours but in detail there are significant differences. They also calculated the energy bands using initial potential approximations corresponding to Li^0F^0 and Li^+F^- and found energy band gaps ($\Gamma_{15} \rightarrow \Gamma_1$) of 15.2 and 14.2 eV, respectively. This difference is of the same sign and magnitude (~1 eV) as found in our calculation. They too found "only a rather small difference between the band structures resulting from these two models." The difference between this calculation and ours may be attributed to their using Hartree–Fock free-ion charge densities and a different exchange approximation in the solid. This appears to be confirmed by Table I of Painter.[25] They further calculated the band structure self-consistently and found that the self-consistent charge densities about each species corresponded quite closely to that about the corresponding free ion. They found $\Gamma_{15} \rightarrow \Gamma_1$ equal to 10.9 eV, which is quite close to our value of 11.3 eV for model II. The top of their valence band is 12.3 eV below the vacuum, which is consistent with the photoemission work.[27]

Painter[25] also calculated the LiF energy bands using the linear-combination-of-atomic-orbital (LCAO) or tight-binding method. He too used both neutral-atom and free-ion charge densities. When he used Hartree–Fock free-atom (-ion) charge densities he obtained values too large for the direct gap but very good agreement with the results of Chaney *et al.*[24] When he used Hartree–Fock–Slater $\alpha = 1$ free-atom charge densities, corresponding to our model I, he obtained $\Gamma_{15}' \rightarrow \Gamma_1$ equal to 12.2 eV, which compares well with our value of 12.55 eV. He finds that the bands have an overall upward shift of about 7 eV in going from a neutral starting configuration to an ionic one. Painter also investigated the dependence of the calculated band gaps on the exchange parameter α and found a surprisingly large variation. Much of this must be attributed to the use of a different exchange approximation in the free atom than was used in the solid.

Drost and Fry[26] used a self-consistent LCAO method to calculate the LiF energy bands. As in the preceding cases, although their bands agree with ours as to general appearance, there are differences in detail. In particular, they find $\Gamma_{15} \rightarrow \Gamma_1$ equal to about 18.3 eV using an exchange parameter $\alpha = 1$. This gap seems large compared with other LCAO calculations using a similar ionic potential and may reflect convergence problems. Including polarization corrections to the band energies, a value of $\alpha = 0.87$ was found to give the best fit to the experimental energy gaps. They found that the self-consistent charge density involved a charge transfer from the F^- ion to the Li^+ ion of less than 0.01 electrons and hence concluded that for all practical purposes the crystal is fully ionic.

We conclude, therefore, that our muffin-tin potential constructed for a Li^+F^- starting configuration provides a reasonable description of the bulk electronic properties of LiF. However, the use of any bulk potential to describe the scattering properties of the surface atoms is always somewhat suspect. Since in LEED we are primarily concerned with scattering events involving large momentum transfer, the portion of the electron–ion-core potential that we probe is primarily determined by the core levels.[37,38] This part of the potential will be little altered by the different geometrical configuration of a surface atom. The position of the zero level between the atomic potentials is more dependent on the local geometry, but exploring the consequences of this is beyond the scope of the present work. The model potential does, however, predict a reasonable photoemission threshold and so surface modifications are perhaps not too extreme.

IV. VIBRONIC AND ELECTRONIC RENORMALIZATION EFFECTS

LEED involves the scattering of fairly high-energy electrons which can create electronic and vibronic excitations in the solid. The renormalization effects introduced by these excitations have been extensively discussed by Duke and Laramore[39–42] and so here we merely review some of the salient features.

The main effect of the lattice vibrations is to renormalize the effective electron–ion-core elastic scattering amplitude making it temperature dependent.[39,40] Although the theory is formulated so as to allow for an asymmetric mode of vibration (e.g., a larger vibrational amplitude perpendicular to the surface than parallel to it), here we shall assume that each ion core has a spherically symmetric mode of vibration which can be characterized by an effective Debye temperature. This is a reasonable approximation in the absence of any detailed experimental study of the temperature dependence of the LEED scattering data. We thus write the renormalized scattering amplitude for the nth ion core as

$$b_n(\vec{k}_2, \vec{k}_1) = \exp[-W(T, \Theta_D^n, M_n)(\vec{k}_2 - \vec{k}_1)^2]\, t_n(\vec{k}_2, \vec{k}_1), \tag{2}$$

where $\vec{k}_1$ is the wave vector of the incident electron, $\vec{k}_2$ is the wave vector of the scattered electron, $t_n(\vec{k}_2, \vec{k}_1)$ is the scattering amplitude for the nth ion core when it is held rigid, and

$$W(T, \Theta_D^n, M_n) = \frac{3\hbar^2}{2M_n k_B \Theta_D^n}\left[\frac{1}{4} + \left(\frac{T}{\Theta_D^n}\right)^2 \times \int_0^{\Theta_D^n/T} dx\, \frac{x}{e^x - 1}\right]. \tag{3}$$

In Eq. (3) T is the temperature of the solid, M_n is the mass of the nth ion core, and Θ_D^n is the Debye temperature characterizing the vibrational amplitude of the nth ion core.

$t_n(\vec{k}_2, \vec{k}_1)$ is specified in terms of the partial-wave phase shifts obtained from the electron–ion-core potential. Only the $l = 0$, 1, and 2 phase shifts shown in Figs. 1 and 2 were used in the present work. The procedure is described in detail in Ref. 3 and explicit expressions for the partial-wave components of $b_n(\vec{k}_2, \vec{k}_1)$ are given there. Values for the bulk Debye temperatures were obtained from the room-temperature x-ray measurements of Witte and Wölfel.[43] These are

$$\Theta_D(\mathrm{Li}) \simeq 720\ ^\circ\mathrm{K} \tag{4a}$$

for the lithium and

$$\Theta_D(\mathrm{F}) \simeq 540\ ^\circ\mathrm{K} \tag{4b}$$

for the fluorine. Both theoretical calculations[44–49] and experimental measurements[50–60] indicate that, in general, surface atoms have a substantially larger vibrational amplitude than those in the bulk. It would be necessary to take this into account in fitting the temperature dependence of the experimental LEED intensity data.[9,40,60] However, at any given temperature the main effect of the larger vibrational amplitude of the surface atoms would be to reduce the intensities of the peaks in the intensity profiles and not change their positions. In view of this and in the absence of any detailed information about the temperature dependence of the LEED intensities, we shall simply take the surface atoms to have the same vibrational amplitude as those in the bulk. The experimental measurements were made at $T \simeq 573\ ^\circ\mathrm{K}$ in order to increase the conductivity of the sample sufficiently to avoid charging the surface by the electron beam.[16] This is the temperature used in evaluating Eq. (3). From the thermal expansion measurements of Yates and Panter[61] we estimate the bulk lattice constant at 573 °K to be about 4.06 Å. We use this value to specify the perfect surface geometrical parameters. Percentage changes in the surface-layer spacing are specified in terms of the 573 °K bulk lattice parameters.

The main effect of the electronic excitations is to renormalize the electron propagator which describes the motion of the beam electrons between successive scatterings by the ion cores.[39,41,62] Although the presence of the surface means that in general the degeneracy between the parallel and perpendicular components of the wave vector is removed,[41,62] in carrying out the partial-wave expansion the propagator was assumed to be spherically symmetric.[39,40] We also assume that the proper self-energy depends only on the energy of the electron and thus write the one-electron propagator as

$$G(\vec{k}, E) = [E - \hbar^2 k^2/2m - \Sigma(E)]^{-1}, \tag{5}$$

where $\Sigma(E)$ is the electronic proper self-energy. $\Sigma(E)$ is complex with the real part relating the effective zero level of energy inside the crystal to the vacuum level and the imaginary part describing the decrease of the number of electrons at the primary-beam energy E due to inelastic processes involving electronic excitations.[39,41]

Bulk-electron-gas calculations indicate that $\mathrm{Re}\Sigma$ varies appreciably with energy for electrons in the LEED energy range.[63,64] However, we regard it as necessary to use a consistent energy zero for both the electron propagator and the effective electron–ion-core potential. As an energy-independent exchange potential was used in the construction of the muffin-tin potentials, we also use an energy-independent value for $\mathrm{Re}\Sigma(E)$. This is taken to be $-V_0$, the distance between the vacuum level and the muffin-tin zero.[3,42] Other workers do not impose this consistency requirement.[2,4] We shall see that a reasonable description of the LiF LEED intensity data can be obtained without treating $\mathrm{Re}\Sigma(E)$ as a free parameter.

The only free parameter in our calculation is the inelastic collision mean free path which specifies $\mathrm{Im}\Sigma(E)$. We write

$$\mathrm{Im}\Sigma(E) = -\frac{\hbar^2}{m\lambda_{ee}}\left(\frac{2mE}{\hbar^2} + \frac{2mV_0}{\hbar^2}\right)^{1/2}, \tag{6}$$

where λ_{ee} is twice the effective-electron mean free path. Estimates of $\mathrm{Im}\Sigma(E)$ have been made for bulk-electron-gas systems[63,65,66] but the applicability of these estimates to the surface region of insulators is questionable. In our calculations we take λ_{ee} to be energy independent. A value of $\lambda_{ee} = 8$ Å appears to give a reasonable description of the data but we also show the effect of larger and smaller values of λ_{ee} on the calculated intensity profiles.

V. LEED INTENSITY PROFILES

In this section we present calculated intensity profiles and compare them with experimental data. The theoretical calculations are for the absolute reflectivity[3] but unfortunately the units of the experimental curves are arbitrary. McRae and Caldwell[16] give only one experimental intensity profile over a fairly extensive energy range. This is for the specular beam at an angle of incidence of 12° with the surface normal. The azimuthal orientation of the beam is along one of the axes of the primitive square lattice of the surface net. We will concentrate primarily on this intensity profile. For $\lambda_{ee} = 12$ Å, six layers were used for the lithium and the fluorine sublattices and for $\lambda_{ee} \leq 8$ Å, five layers were used in each sublattice.

We first consider a model which treats the surface as if it were simply a truncation of an idealized perfectly periodic bulk solid. In Fig. 5 calculations of the LEED intensity profiles using both potential I and potential II are compared with the experimental measurements of McRae and Caldwell.[16] The dotted arrows indicate the positions of several of the prominent experimental peaks. Figure 5(a) shows an intensity profile calculated using potential I with $V_0 = 18$ eV. The three prominent peaks that appear can be classified as primary Bragg peaks.[67,68] These lie about 7 eV lower in energy than the corresponding experimental peaks. Note also that there is no peak corresponding to the prominant 9-eV peak observed experimentally. Holland *et al.*[18] used $V_0 = 0$ in their s-wave calculations in order to produce a peak near 9 eV. In Fig. 5(b) we show an intensity profile calculated using the phase shifts from potential I, but with $V_0 = 0$. This does produce a peak near 9 eV but now the other peaks are considerably higher in energy than their experimental counterparts. Holland *et al.*[18] try to finesse this point by arguing that V_0 really is varying appreciably with electron energy and that at 150 eV V_0 should be about 10–15 eV. The main difficulty is that we would expect the energy-independent local exchange used in determining V_0 to be more appropriate at the lower electron energies and not at the higher energies. In Fig. 5(c) we show an intensity profile calculated using potential II with $V_0 = 11.6$ eV. There is good correlation between the three prominent peaks and their experimental counterparts. The theoretical curve also shows a shoulder at about 55 eV where experimentally there is a resolved peak. However, the theoretical calculation does not produce a peak near 9 or 85 eV. Potential II thus appears to do a more adequate job of describing the experimental data although the comparison between Figs. 5(c) and 5(d) is by no means totally satisfactory. The curves in Figs. 5(a) and 5(c) are essentially only shifted with respect to one another. This shift is due to the different values of V_0 for potentials I and II, which in turn is due to the different ionicities of the starting configuration. This indicates that unless V_0 is treated as an adjustable parameter, it will be important to properly account for the charge transfer between the adsorbate and the substrate in constructing potentials for calculations of LEED intensities from adsorbed overlayers. However, proposed energy-averaging techniques[12,13] for obtaining the two-dimensional structure of the adsorbed overlayer should not be too sensitive to this feature of the potential.

The question arises as to whether the experimental peak at 9 eV could be due to an intralayer resonance[69,70] scattering which an incorrect choice of λ_{ee} has masked in the full calculation. Increas-

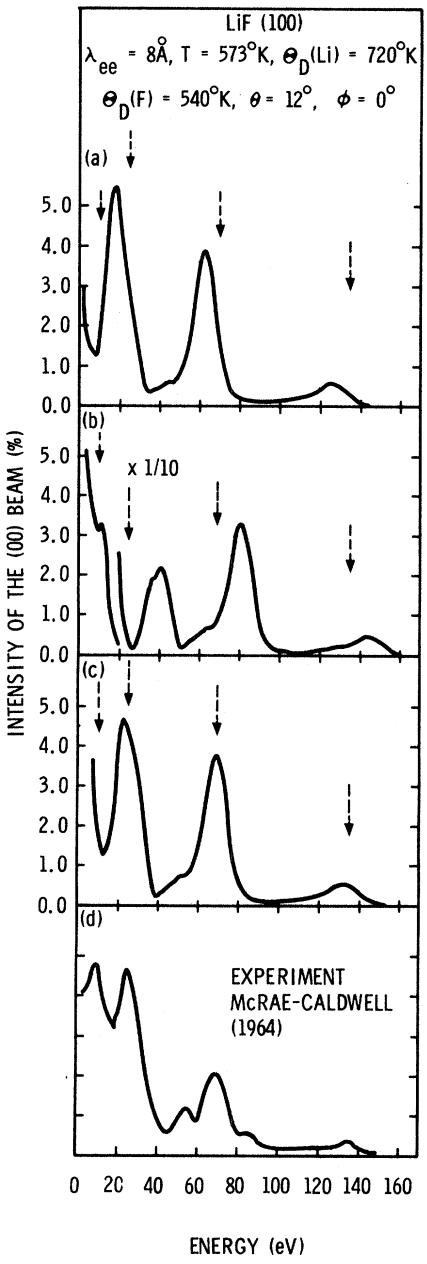

FIG. 5. Comparison between intensity profiles for the specular beam calculated using potential I and potential II and the experimental work of McRae and Caldwell (Ref. 16). The polar angle is $\theta = 12°$, and the azimuthal angle φ is measured relative to an axis of the primitive square lattice of the surface net. The parameters used in the calculation are indicated in the figure. The theoretical calculations are for the absolute reflectivity but the units of the experimental curve are arbitrary. (a) shows a calculation using potential I with $V_0 = 18$ eV. (b) shows a calculation using the phase shifts from potential I but with V_0 artificially set equal to zero. (c) shows a calculation using potential II with $V_0 = 11.6$ eV. The dotted arrows indicate the positions of some of the prominent peaks observed experimentally.

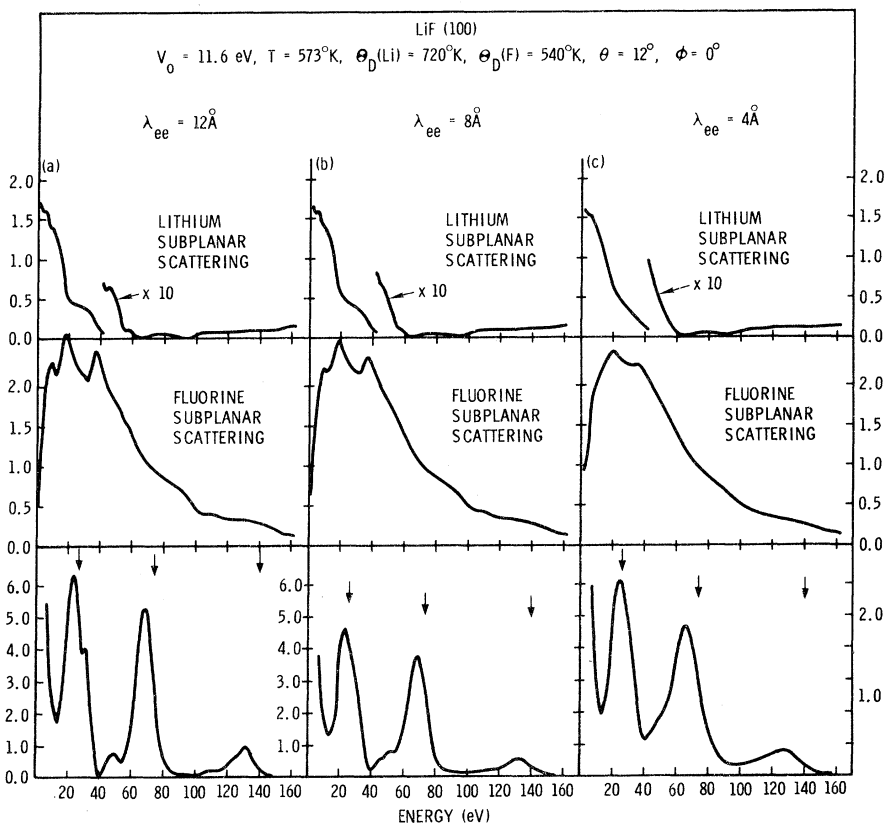

FIG. 6. Calculated scattering cross sections for the lithium and the fluorine subplanes and the calculated intensity profiles (bottom row) for various values of the inelastic mean free path parameter λ_{ee}. (a) corresponds to λ_{ee} = 12 Å, (b) to λ_{ee} = 8 Å, and (c) to λ_{ee} = 4 Å. The other parameters used in the calculation are indicated in the figure. The units of the subplanar cross sections are arbitrary but the intensity profiles are for the absolute reflectivity and are in percent. Model potential II was used for the calculation. The arrows mark the kinematical Bragg positions using V_0 = 11.6 eV.

ing λ_{ee} increases the amount of structure in the subplanar scattering cross sections. However, it also increases the strong multiple scattering between layers which may reduce the importance of the subplanar resonance structure in the full calculation. On the other hand, decreasing λ_{ee} makes the scattering from the top layer more important but reduces the resonance structure in the intraplanar cross section. In Fig. 6 we show the intralayer scattering cross sections for both the lithium and the fluorine subplanes as well as the calculated intensity profiles for different values of λ_{ee}. The fluorine subplanar scattering cross section exhibits a sharp rise to a local maximum near 10 eV for λ_{ee} = 12 and 8 Å, but this is not reflected in a corresponding peak in the intensity profiles. The lithium subplanar scattering cross section is essentially a decreasing function of energy in this energy range. Although using λ_{ee} = 12 Å resolves the multiple scattering peak at 50 eV which is just a shoulder for $\lambda_{ee} \leq 8$ Å, it also produces structure near 30 eV which is not seen experimentally. Simply varying λ_{ee} does not bring the theoretical curves into better correspondence with the experimental results. The intensities of the peaks in the calculated intensity profiles are different; but even if absolute intensity measurements were experimentally available, one would still have to take account of the decrease in intensity due to the larger vibrational amplitude of the surface atoms in order to determine the best value for λ_{ee}.

We next investigate the effect of various changes in the geometrical parameters of the surface region on the calculated intensity profiles. The geometrical effects that we will be concerned with are schematically illustrated in Fig. 7. According to the calculations of Benson *et al.*[28–30] the (100) faces of the alkali halides not only can have an upper-layer spacing different from the bulk layer spacing, but also the lithium and the fluorine sublayers in the upper layer can be contracted toward the bulk by different amounts. This results

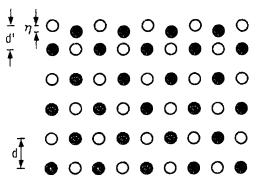

FIG. 7. Schematic illustration of parameters specifying the surface reconstruction for the (100) face of lithium fluoride. d' is the spacing between the second layer and "least-contracted" sublayer in the top layer. η is the separation between the sublayers in the top layer. d is the bulk layer spacing.

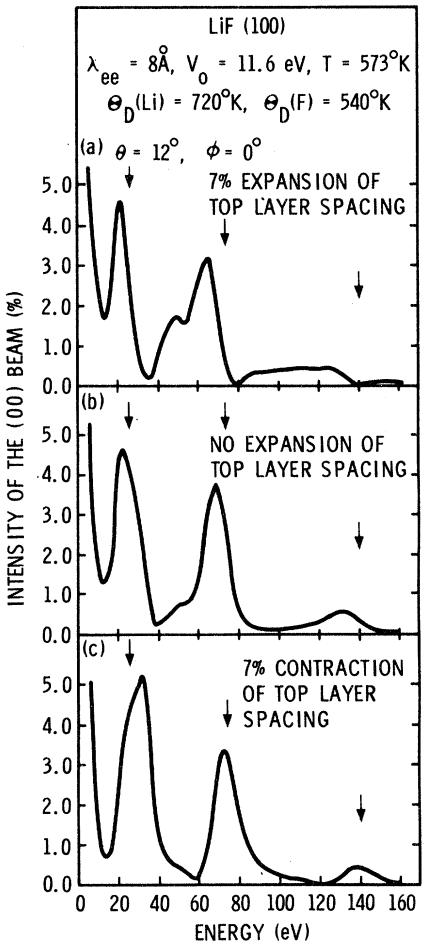

FIG. 8. Effect of a uniform expansion or contraction of the upper-layer spacing (i.e., $\eta = 0$, $d' \neq d$) on the calculated intensity profiles. The calculations are for the absolute reflectivity and use model potential II and the parameters indicated in the figure. The arrows mark the kinematical Bragg positions using $V_0 = 11.6$ eV.

in the lithium and fluorine sublayers no longer lying in the same plane. The same type of distortion is present in the second, third, etc., layers, but its relative magnitude dies out rapidly with distance from the surface. For simplicity we use a model where only the surface layer is affected. The parameters d' and η which we use to specify the surface distortion are illustrated in Fig. 7. In an early calculation for LiF (100) in which only the top layer was allowed to relax, Benson[28] found a value of $\eta \simeq 0.12$ Å, with the Li^+ sublayer being the most contracted towards the bulk region. However, subsequent work[29,30] involving the relaxation of more than one layer failed to converge for LiF (100). We also note that the work of Benson *et al.*[28-30] ignores vibronic effects and hence its quantitative applicability to high-temperature measurements is doubtful. Thus we shall systematically investigate the effects of various aspects of the surface distortion in order to see their individual as well as collective effect on the calculated intensity profiles.

In Fig. 8 we show the effect of a uniform expansion or contraction of the upper-layer spacing, i.e., $\eta = 0$, $d' \neq d$. In Fig. 8(a) $d' = 1.07d$. The first two primary Bragg peaks have shifted to lower energy and the intensity of the third peak has been spread over such a large energy range that a well-defined maximum is no longer present. The intensity of the secondary structure near 50 eV has been considerably enhanced. In Fig. 8(c) $d' = 0.93d$. The primary Bragg peaks have shifted to higher energies and have high-energy tails. The secondary structure near 50 eV has disappeared into the middle Bragg peak. Since $d = 2.03$ Å, the distance by which the upper layer was shifted in each case is 0.14 Å. The modifications of the intensity profiles due to uniform changes in the upper-layer spacing are quite similar to those

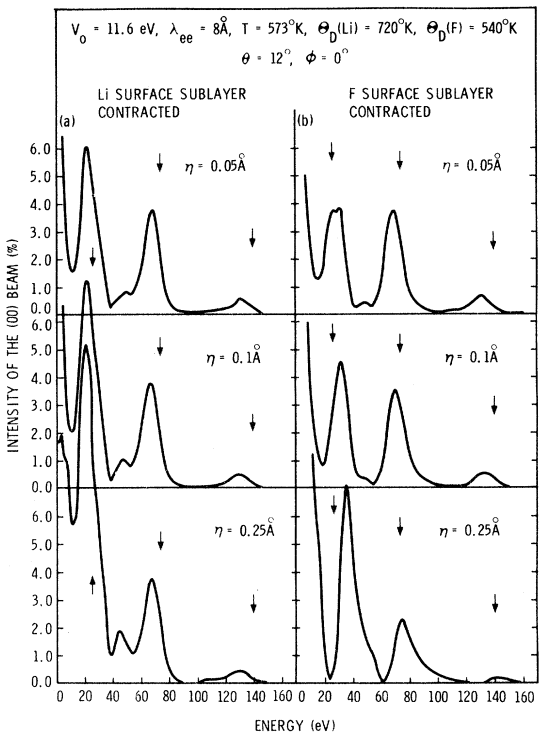

FIG. 9. Effect of a separation between the top lithium and fluorine sublayers on the calculated intensity profiles (i.e., $d' = d$, $\eta \neq 0$). The calculations are for the absolute reflectivity and use model potential II and the parameters indicated in the figure. (a) shows the effect of contracting the lithium sublayer towards the bulk by increasing amounts, and (b) shows the corresponding curves with the fluorine sublayer being contracted towards the bulk. The arrows mark the kinematical Bragg positions using $V_0 = 11.6$ eV.

observed previously[3] in calculated intensity profiles for Al (100) and Al (110). There is no tendency to produce an extra peak near 9 eV.

In Fig. 9 we show the effect of a separation between the top lithium and fluorine sublayers on the calculated intensity profiles. We take $d = d'$ and $\eta \neq 0$. Figure 9(a) shows the calculated curves when the top lithium sublayer is contracted towards the bulk by various amounts, and Fig. 9(b) shows corresponding curves when the top fluorine sublayer is contracted towards the bulk. Note that although the symmetry of the system is broken in exactly the same way when either the lithium or the fluorine sublayer is contracted, the calculated curves are noticeably different for the two cases. This is due to the quite different scattering properties of the component species. Not only are the details of the secondary structure different, but also the behavior of the primary Bragg peaks is quite different. Contracting the lithium sublayer shifts the peaks to lower energies while contracting the fluorine sublayer shifts the peaks to higher energies. Most importantly, we note that with a 0.25-Å contraction of the top lithium sublayer an additional peak has developed at very low energies. Also the secondary structure near 50 eV is clearly resolved. Referring back to Fig. 5(d), we see that all the peaks are now at too low an energy. However, looking at Fig. 9(c) we see that if we would make $d' < d$ this would have the effect of shifting the peaks in the calculated intensity profile to higher energy. In connection with this we note that Benson's calculation[28] predicted that d' would be about 0.1 Å less than d.

In Fig. 10 we show the combined effect of $d' \neq d$ and $\eta \neq 0$ with the top lithium sublayer being contracted towards the bulk more than the top fluorine sublayer. Corresponding curves are shown for the perfect surface and the experimental measurement of McRae and Caldwell[16] is also shown for purposes of comparison. The calculation for the specular beam using $\eta = 0.25$ Å and $d' = 1.93$ Å corresponds much more closely to the experimental data than the calculation assuming a perfect surface. The observed peak at about 9 eV is present in the calculation and the positions of the three Bragg peaks agree quite well with the positions of the corresponding experimental peaks. However, the secondary structure between the first two Bragg peaks is not adequately described by the calculation since it is at about 45 eV in the calculated curve but is at about 55 eV in the experimental measurement. Also the second Bragg peak in the calculated intensity profiles exhibits a high-energy tail and not the resolved peak at about 85 eV observed experimentally. Although experimental intensity profiles for the $(0\bar{1})$ and $(\bar{1}\,\bar{1})$ beams have not yet been measured, we calculated these intensity profiles also to see if there were any dramatic differences between the predictions of the two surface models. There are differences between the two sets of calculated intensity profiles for the nonspecular beams, but clearly the most dramatic effect involves the existence of the 9-eV peak for the (00) beam.

Curves were also calculated using $\eta = 0.25$ Å and $d' = 1.93$ Å but with the top fluorine sublayer being contracted the greater amount toward the bulk. The calculated curves (not shown) did not produce the peak at 9 eV and so the experimental data definitely seem to discriminate in favor of the lithium sublayer being contracted the greater amount toward the bulk. McRae and Caldwell[16] postulated that the existence of the 9-eV peak was due to the symmetry breaking caused by the separation of the top lithium and fluorine sublayers. However, they did not pursue the matter in any detail. Our calculations show that it is not sufficient just to break the symmetry in this way, but it is neces-

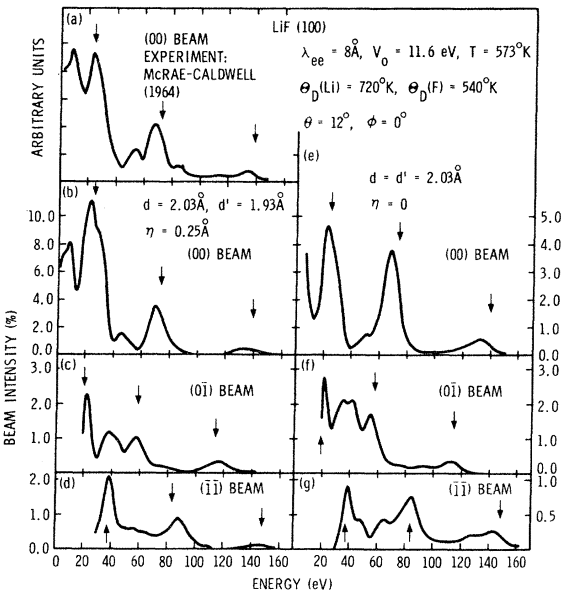

FIG. 10. Calculated intensity profiles for a separation between the top lithium and fluorine sublayers compared with the experimental measurements of McRae and Caldwell (Ref. 16) and with calculated intensity profiles for a perfect surface. (a) shows the experimental work of McRae and Caldwell, (b)–(d) show the calculated intensity profiles for the reconstructed surface with the lithium sublayer contracted the greater amount toward the bulk, and (e)–(g) show the calculated intensity profiles for a perfect planar surface. The calculations are for the absolute reflectivity and use model potential II and the parameters indicated in the figure. The beams are labeled according to the primitive square lattice of the surface net where the incident beam is oriented along the positive x axis. The arrows mark the kinematical Bragg positions using $V_0 = 11.6$ eV.

sary that the lithium sublayer be contracted the greater amount toward the bulk.

The agreement between theory and experiment shown in Figs. 10(a) and 10(b) is not perfect, but it is certainly better than the agreement between Figs. 10(a) and 10(e). This argues strongly for the existence of the surface distortion predicted by Benson *et al.* [28–30] and to our knowledge is the first evidence for this effect. The separation between the lithium and the fluorine sublayers would cause an additional electric field to be present at the surface. The size of this field would depend upon the details of the charge distribution. If one assumes that the charges involved are spread into uniform sheets separated by 0.25 Å, then the potential difference in passing between the two sheets is about 5.5 eV. This is, no doubt, an overestimate of the actual potential difference in the crystal, but it is not surprising that calculations which ignore this effect do not reproduce the fine details of the experimental curves. We also note that the degree of modification of the intensity profiles produced by any alteration of the surface geometrical parameters depends on the relative strengths of the scattering between the surface and bulk regions. [3] That is, the quantitative numbers obtained for d' and η certainly depend on the assumed values of λ_{ee} and the vibrational amplitudes of the surface atoms. However, the qualitative aspects of the interpretation will not be affected by these uncertainties.

McRae and Caldwell [16] also presented curves showing the detailed behavior of the specular beam intensities between 10 and 50 eV for many angles of incidence. A comparison between some of these experimental curves and the predictions of the two surface models is shown in Fig. 11. Note that the intensities are plotted on a logarithmic scale to show the fine details of the intensity variation. McRae and Caldwell [16] show intensity profiles between 6° and 34° in 1° increments for this azimuth but we use only about a 5° sampling grid in Fig. 11. On a logarithmic intensity scale the comparison between theory and experiment is quite poor for both models of the crystal surface. One might argue that for $\theta = 5°$ and 10° the reconstructed-surface model compares slightly better with experiment because the width of the predicted maximum is less than for the perfect-surface case. However, for $\theta \geq 15°$ the predictions of both surface models bear little if any resemblance to the experimental data. McRae and Caldwell [16] give a similar set of curves for this energy range for the $\varphi = 45°$ azimuth. A few curves were calculated for this azimuth using both surface models but the degree of correspondence was about the same as shown in Fig. 11 and so it was not thought worthwhile to construct a detailed figure for this case.

Holland *et al.* [18] make a comparison between their s-wave calculations for the specular beam and the detailed experimental data of McRae and Caldwell [16] for the two azimuths at 3° intervals in θ. They claim a general correspondence between the calculated and experimental curves regarding certain trends with increasing θ. However, there is certainly no detailed agreement. s-wave calculations were not performed for a reconstructed surface but Holland *et al.* [18] appear to believe that a reconstructed surface would only worsen the

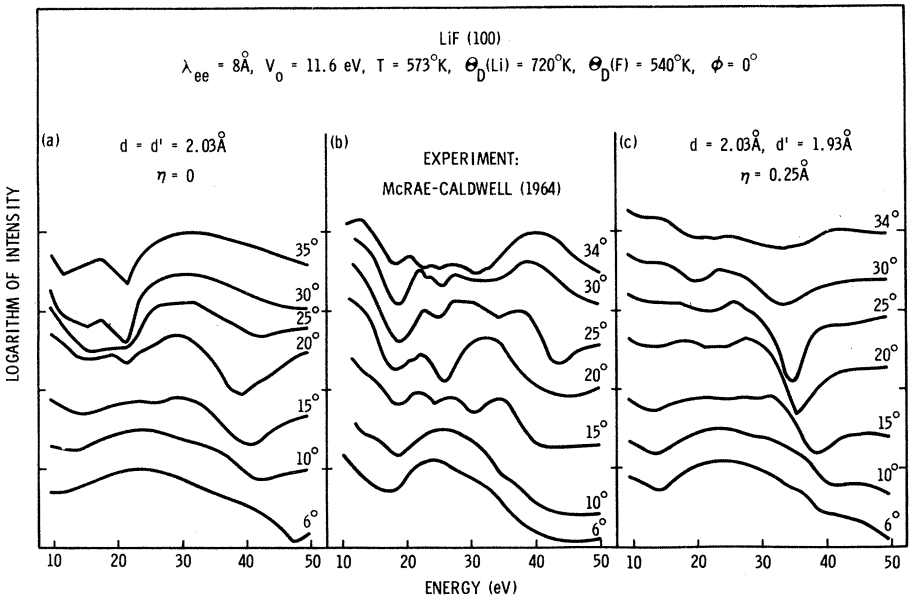

FIG. 11. Comparison between the experimental measurements of McRae and Caldwell (Ref. 16) for the specular beam (a) and calculated intensities for a perfect surface (b) and for the reconstructed surface (c). The intensities are in arbitrary units on a logarithmic scale and the curves are labeled by the polar angle θ. The intensity calculations use model potential II and the parameters indicated in the figure.

agreement between their calculations and the experimental results.

Hirabayashi[17] also uses an s-wave model to calculate the intensities for the specular beam between 10 and 50 eV for polar angles of $\theta = 6°$, 10°, 15°, 20°, and 25°. He does not show the experimental data of McRae and Caldwell[16] on the same scale as the calculated intensities but one can safely say that there is no detailed correspondence between theory and experiment.

Including the higher partial waves has not resulted in complete agreement with experiment, but the agreement was sufficiently improved that the effect of surface reconstruction could be identified in the experimental intensity profiles. Both previous s-wave calculations[17,18] appear to have missed this effect. We also note that it is the quite different scattering properties of the constituents which allowed us to ascertain whether the lithium or the fluorine sublayer was contracted the greater amount towards the bulk. The extent to which this could be simulated in an s-wave calculation is unclear.

In earlier work on aluminum[3] it was noticed that the model calculations appeared to work better at the smaller angles of incidence. In an effort to motivate more experimental work we present in Fig. 12 calculated intensity profiles for the specular and nonspecular beams at normal incidence for the two different models of the surface. Comparing the intensity profiles for the (00) beam it seems safe to say that for $\varphi = 0°$ and for $\theta \lesssim 12°$, the reconstructed-surface model will produce a low-energy peak near 9 eV but that the perfect-surface model will not. This will be an important feature in using LEED to identify a separation between the top lithium and fluorine sublayers. Very high reflectivities are shown in the calculated curves. These may be artificially large since the electron self-energy renormalization effects were assumed to start at the center of the outermost ion cores. Since the electrons extend outside this distance, it may be more realistic to include the renormalization effects at a larger distance. This would affect the magnitude of the calculated intensity profiles but not their shape. The features in the nonspecular beams are enough different for the two surface models that they also will be useful in checking the existence of the sublayer separation.

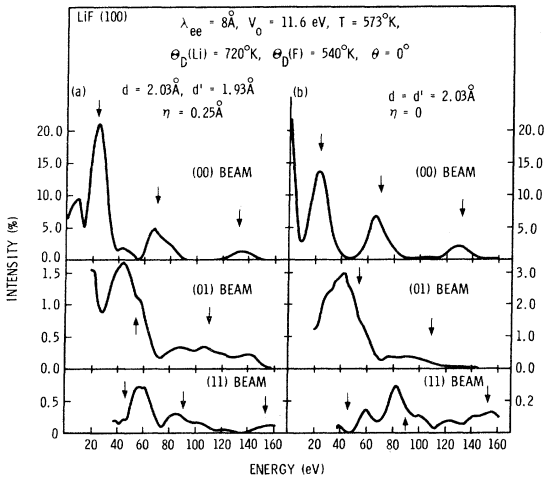

FIG. 12. Comparison between the predicted intensity profiles at normal incidence using in (a) a surface model with a 0.25-Å separation between the top lithium and fluorine sublayers with the lithium sublayer being more contracted towards the bulk and in (b) an idealized planar surface. The calculations are for the absolute reflectivity and use model potential II and the parameters indicated in the figure. The beams are labeled according to the primitive square net of the surface layer and the arrows mark the kinematical Bragg positions using V_0 = 11.6 eV.

VI. SUMMARY AND CONCLUSIONS

In this paper we broached some of the questions that arise when one calculates LEED intensities for a multicomponent system. One problem involves taking proper account of the charge transfer between the component species. This was investigated by calculating the electronic energy bands and LEED intensity profiles for two different sets of electron–ion-core potentials: One set was constructed from Li^0 and F^0 free-atom charge densities and the other set was constructed from Li^+ and F^- free-ion charge densities. It was found that the main difference between the two sets of potentials was the position of the effective zero level relative to the vacuum. The two potentials gave rather similar band gaps but the photoemission threshold[27] clearly favored the Li^+F^- form of the potential. Just like photoemission, LEED is sensitive to the positioning relative to the vacuum of the effective ion-core potentials of the solid and the calculated intensity profiles using the Li^+F^- form of the potential agreed much better with experimental measurements. Hence LEED measurements may shed some light on this aspect of potentials constructed for band structure calculations. However, like photoemission, LEED is surface sensitive and the extent to which measurements are applicable to bulk potential properties is not clear. The positions of the peaks in the calculated intensity profiles were quite sensitive to the charge transfer between the component species and presumably this will also be the case for adsorbed overlayer systems.

On the other side of the coin, fitting the low-lying electronic properties via a band-structure calculation gave us a reasonable starting point for electron–ion-core potentials to be used in LEED.

Using the model potential constructed from Li^+F^- charge densities we investigated the surface properties of LiF (100). We found that certain features of the experimental measurements of McRae and Caldwell[16] seemed to indicate that at 573 °K the top lithium and fluorine sublayers were separated by about 0.25 Å with the lithium sublayer being contracted the greater amount towards the bulk. This type of reconstruction for the (100) face of the alkali halides has been predicted by Benson *et al.*,[28-30] but to our knowledge this is the first evidence for the effect. In order to motivate additional experimental work on this system, intensity profiles were calculated for the nonspecular beams for the beam orientation of McRae and Caldwell[16] and also for a normally incident beam. The calculations were performed both for the reconstructed surface and the perfect surface and diagnostic features subject to experimental test were pointed out. In our analysis we tacitly assumed that the surface was planar and had the same chemical stoichiometry as the bulk. The use of Auger-electron spectroscopy[71] or appearance-potential spectroscopy[72] in future work would provide a test for surface chemical contamination but the extent to which they would indicate a lithium- or fluorine-rich surface is unclear. Analysis of the angular distribution of the scattered intensity would characterize the surface morphology.[73,74]

In the event that subsequent experimental work also indicates that the surface is rearranged, the calculations could be redone using more accurate values for λ_{ee} and the vibrational amplitude of the surface atoms (these could be estimated from the temperature dependence of the LEED intensities[42]), and perhaps also using potentials constructed from overlapping ionic charge densities with a geometric configuration corresponding to the rearranged surface. This would yield more accurate values for d' and η.

Note added in proof: A paper by Benson and Claxton[75] using a shell model instead of a point-ion model predicts a differential relaxation for the top layer of LiF (100) of the type that we described here. Benson and Claxton[75] also find that the second layer is significantly distorted. We would like to thank Dr. G. P. Alldredge for calling this paper to our attention.

ACKNOWLEDGMENTS

We would like to thank Dr. E. G. McRae for helpful discussions regarding the experimental data and D. G. Schreiner for his assistance in plotting the experimental data.

*Work supported by the U. S. Atomic Energy Commission.

[1]J. A. Strozier and R. O. Jones, Jr., Phys. Rev. Lett. **25**, 516 (1970); Phys. Rev. B **3**, 3228 (1971).

[2]S. Y. Tong and T. N. Rhodin, Phys. Rev. Lett. **25**, 711 (1971).

[3]G. E. Laramore, C. B. Duke, A. Bagchi, and A. B. Kunz, Phys. Rev. B **4**, 2058 (1971); G. E. Laramore and C. B. Duke, Phys. Rev. B **5**, 267 (1972).

[4]D. W. Jepsen, P. M. Marcus, and F. P. Jona, Phys. Rev. Lett. **26**, 1365 (1971); Phys. Rev. B **5**, 3933 (1972).

[5]J. B. Pendry, J. Phys. C **4**, 2514 (1971).

[6]S. Andersson and J. B. Pendry, J. Phys. C **5**, L41 (1971).

[7]F. Jona, J. A. Strozier, Jr., J. Kumar, and R. O. Jones, Phys. Rev. B **6**, 407 (1972).

[8]R. H. Tait, S. Y. Tong, and T. N. Rhodin, Phys. Rev. Lett. **28**, 553 (1972).

[9]G. E. Laramore, Phys. Rev. B **6**, 2950 (1972).

[10]J. W. May, Adv. Catal. Relat. Subj. **21**, 152 (1970).

[11]P. J. Estrup and E. G. McRae, Surf. Sci. **25**, 1 (1971).

[12]C. W. Tucker, Jr. and C. B. Duke, Surf. Sci. **23**, 411 (1970); J. Vac. Sci. Technol. **8**, 5 (1971).

[13]C. B. Duke and G. E. Laramore, Surf. Sci. **30**, 659 (1972).

[14]M. G. Lagally, T. C. Ngoc, and M. B. Webb, Phys. Rev. Lett. **26**, 1557 (1971); J. Vac. Sci. Technol. **9**, 645 (1972).

[15]T. C. Ngoc, M. G. Lagally, and M. B. Webb, Surface Sci. (to be published).

[16]E. G. McRae and C. W. Caldwell, Jr., Surf. Sci. **2**, 509 (1964).

[17]K. Hirabayashi, J. Phys. Soc. Jap. **30**, 211 (1971).

[18]B. W. Holland, R. W. Hannum, and A. M. Gibbons, Surf. Sci. **25**, 561 (1971).

[19]L. Pauling, *The Nature of the Chemical Bond* (Cornell U. P., Ithaca, N. Y., 1960).

[20]J. C. Phillips and J. A. Van Vechten, Phys. Rev. B **2**, 2147 (1970); Phys. Rev. B **2**, 2160 (1970).

[21]J. C. Slater, Phys. Rev. **51**, 846 (1937); T. L. Loucks, *Augmented Plane Wave Method* (Benjamin, New York, 1967); J. O. Dimmock, in *Solid State Physics*, edited by F. Seitz, D. Turnbull, and H. Ehrenreich (Academic, New York, 1971), Vol. 26.

[22]L. F. Mattheiss, J. H. Wood, and A. C. Switendick, *Methods of Computational Physics*, edited by B. Alder, S. Fernbach, and M. Rotenberg (Academic, New York, 1968), Vol. 8.

[23]L. J. Page and E. H. Hygh, Phys. Rev. B **1**, 3472 (1970).

[24]R. C. Chaney, E. E. Lafon, and C. C. Lin, Phys. Rev. B **4**, 2734 (1971).

[25]G. S. Painter, in *Proceedings of the International Symposium on Atomic, Molecular, and Solid State Theory and Quantum Biology, 1971*, edited by P. Löwdin (Interscience, New York, 1971), p. 501.

[26]D. M. Drost and J. L. Fry, Phys. Rev. B **5**, 684 (1972).

[27]S. W. Duckett and P. H. Metzger, Phys. Rev. **137**, A953 (1965).

[28]G. C. Benson, J. Chem. Phys. **35**, 2113 (1961).

[29]G. C. Benson, P. I. Freeman, and E. Dempsey, J. Chem. Phys. **39**, 302 (1963).

[30]G. C. Benson and K. S. Yun, in *The Solid-Gas Interface*, edited by E. A. Flood (Marcel Dekker, New York, 1967), Chap. 8.

[31]F. Herman and S. Skillman, *Atomic Structure Calculations* (Prentice-Hall, Englewood Cliffs, N. J., 1963).

[32]V. Ern and A. C. Switendick, Phys. Rev. **137**, A1927 (1965).

[33]J. C. Slater, Phys. Rev. **81**, 385 (1951).

[34]A. Milgram and M. Givens, Phys. Rev. **125**, 1506 (1962).

[35]D. M. Roessler and W. C. Walker, J. Phys. Chem. Solids **28**, 1507 (1967).

[36]C. Gout and F. Pradal, J. Phys. Chem. Solids **29,** 581 (1968).
[37]J. S. Schilling and M. B. Webb, Phys. Rev. B **2,** 1665 (1970).
[38]G. E. Laramore, J. Vac. Sci. Technol. **9,** 625 (1972).
[39]C. B. Duke and G. E. Laramore, Phys. Rev. B **2,** 4765 (1970).
[40]G. E. Laramore and C. B. Duke, Phys. Rev. B **2,** 4783 (1970).
[41]C. B. Duke and G. E. Laramore, Phys. Rev. B **3,** 3183 (1971).
[42]G. E. Laramore, Phys. Rev. B **6,** 1097 (1972).
[43]H. Witte and E. Wölfel, Rev. Mod. Phys. **30,** 51 (1958).
[44]M. Rich, Phys. Lett. **4,** 153 (1963).
[45]A. A. Maradudin and J. Melgailis, Phys. Rev. **133,** A1188 (1964).
[46]R. F. Wallis, B. C. Clark, and R. Herman, in *The Structure and Chemistry of Solid Surfaces*, edited by G. A. Somorjai (Wiley, New York, 1969), p. 17-1.
[47]R. E. Allen and F. W. deWette, Phys. Rev. **179,** 873 (1969).
[48]R. E. Allen, F. W. deWette, and A. Rahman, Phys. Rev. **179,** 887 (1969).
[49]T. S. Chen, G. P. Alldredge, F. W. deWette, and R. E. Allen, Phys. Rev. B **6,** 623 (1972).
[50]A. U. McRae and L. H. Germer, Phys. Rev. Lett. **8,** 489 (1962).
[51]A. U. McRae, Surf. Sci. **2,** 522 (1964).
[52]E. R. Jones, J. T. McKinney, and M. B. Webb, Phys. Rev. **151,** 476 (1966).
[53]J. T. McKinney, E. R. Jones, and M. B. Webb, Phys. Rev. **160,** 523 (1967).
[54]R. M. Goodman, H. H. Farrell, and G. A. Somorjai, J. Chem. Phys. **48,** 1046 (1968).
[55]J. M. Morabito, Jr., R. F. Steiger and G. A. Somorjai, Phys. Rev. **179,** 638 (1969).
[56]D. P. Woodruff and M. P. Seah, Phys. Lett. A **30,** 263 (1969).
[57]S. Andersson and B. Kasemo, Solid State Commun. **8,** 1885 (1970).
[58]D. Tabor and J. Wilson, Surf. Sci. **20,** 203 (1970).
[59]D. Tabor, J. M. Wilson, and T. Bastow, Surf. Sci. **26,** 471 (1971).
[60]A. Ignatiev, T. N. Rhodin, S. Y. Tong, B. I. Lundqvist, and J. B. Pendry, Solid State Commun. **9,** 1851 (1971).
[61]B. Yates and C. H. Panter, Proc. Phys. Soc. Lond. **80,** 373 (1962).
[62]P. J. Feibelman, C. B. Duke, and A. Bagchi, Phys. Rev. B **5,** 2436 (1972).
[63]See, for example, L. Hedin and S. Lundqvist, in *Solid State Physics*, edited by F. Seitz, D. Turnbull and H. Ehrenreich (Academic, New York, 1969), Vol. 23.
[64]See, also, Refs. 1, 2, and 4 for a discussion of this point.
[65]J. J. Quinn, Phys. Rev. **126,** 1453 (1962).
[66]L. Kleinman, Phys. Rev. B **3,** 2982 (1971).
[67]In the strictest sense when multiple scattering is present one cannot speak of Bragg peaks. The kinematical Bragg condition is reflected in the intensity profiles only as an envelope for the multiple scattering peaks. However, in a weak scattering material such as LiF, there are prominent peaks near the kinematical Bragg positions, and we shall, following the usual nomenclature, refer to these as Bragg peaks. This point is discussed in some detail in Ref. 68.
[68]C. W. Tucker, Jr. and C. B. Duke, Surf. Sci. **24,** 31 (1971).
[69]This terminology arises from the order in which the multiple scattering renormalizations are carried out. We first sum all scattering events lying within a given subplane of equivalent ion cores and then sum all scattering events between subplanes. See Refs. 39, 40, and 70 for a discussion of this point.
[70]J. L. Beeby, J. Phys. C **1,** 82 (1968).
[71]See, for example, E. N. Sickafus and H. P. Bonzel, in *Recent Progress in Surface Science*, edited by J. F. Danielli, K. G. A. Pankhurst, and A. C. Riddiford (Academic, New York, 1970).
[72]R. L. Park, J. E. Houston, and D. G. Schreiner, Rev. Sci. Instrum. **41,** 1810 (1970).
[73]G. E. Laramore, J. E. Houston, and R. L. Park, J. Vac. Sci. Technol. **10,** 196 (1973).
[74]J. E. Houston, G. E. Laramore, and R. L. Park, Surface Sci. **34,** 477 (1973).
[75]G. C. Bensen and T. A. Claxton, J. Chem. Phys. **48,** 1356 (1968).